Journal of South American Earth Sciences 31 (2011) 81–92

Contents lists available at ScienceDirect

Journal of South American Earth Sciences

journal homepage: www.elsevier.com/locate/jsames

Characterization of a loess–paleosols section including a new record of the last interglacial stage in Pampean plain, Argentina

Ofelia Tófalo [a,*], María Julia Orgeira [a,b], Rosa Compagnucci [b,c], María Susana Alonso [a,b], Adriana Ramos [d]

[a] Departamento Cs. Geológicas, FCEN, Universidad de Buenos Aires, Pabellón II, Ciudad Universitaria, 1428 Buenos Aires, Argentina
[b] CONICET, Argentina
[c] Departamento Cs. de la Atmósfera y de los Océanos, FCEN, UBA, Argentina
[d] INGEIS, UBA/CONICET, Buenos Aires, Argentina

ARTICLE INFO

Article history:
Received 17 February 2010
Accepted 4 September 2010

Keywords:
Sedimentary-pedogenetic sequence
MIS 5
Last interglacial paleoclimate
Chaco-Pampean Basin

ABSTRACT

A new record of the Marine Isotopic Stage 5, the last Interglacial Stage before present is presented in this paper. Sedimentological, micromorphological, trace elements analyses (Rb–Sr) and magnetic polarity determination were performed on Buenos Aires and Ensenada Formation (Late Cenozoic) deposits in the southern Chaco-Pampean Basin (Argentina). This work aims to unravel paleoclimatic and paleoenvironmental information from the analyzed data.

The studied deposits encompass a complex and cyclic 8 m-thick sedimentary-pedogenetic sequence formed by loessic sediments and paleosols with volcano-pyroclastic provenance.

Four tabular units, with net base and top, were defined from erosion surfaces.

An OSL age >126 kyr was obtained from the upper middle part of unit B, which suggests that this unit as well as unit C, could have developed during the latest interglacial stage, equivalent to MIS 5.

The occurrence of calcretes indicates periods of little clastic supply and seasonal arid or semiarid climate while iron oxides, smectites and illite-bearing pedogenetic calcretes point to annual rain rates between 100 and 500 mm. No calcretes of any origin occur in present soils of the same zone. According to our proposed interpretation of the available data, climate during MIS 5 was drier than today. The drier conditions may have been related to lower temperatures during summer.

1. Introduction

Several global warming have taken place because of natural causes during Cenozoic times. Relationship among stable isotopes ($^{18}O/^{16}O$, $^{13}C/^{12}C$, and $^{2}H/^{1}H$) measured on sediments from seafloor and ice cores, are a modern tool for paleoclimatic reconstructions. Based upon stable oxygen isotope studies performed on planktonic foraminifera, Chapman and Shackleton (1998) set an isotopic stages chronology for the last 150 kyr, in which warm (interglacial) and cold (glacial) periods can be distinguished in a millennial scale. The last interglacial stage, before present is the so-called Marine Isotopic Stage 5 (MIS 5). This seems to have lasted from around 125 to 75 kyr, with maximum temperature values higher than present ones, and medium global sea level between 4 and 6 m higher than at present time (Siddall et al., 2007).

The paleoclimatic evidence and climate models simulate arctic summer warming of up to 5 °C during this warm period. The warming was even larger over Eurasia and northern Greenland, whereas the summit of Greenland was calculated to be 2–5 °C higher than present (Jansen et al., 2007).

Careful assessment of this warm isotopic stage, including its starting, evolution and ending should provide relevant information on future climatic scenarios.

The attempts to typify climatic paleo-conditions at medium latitudes of South America during global warming periods, become crucial because it allows to determine the changes in atmospheric circulation patterns with time.

Studies on the Stage 5 record are actually scarce in South America, where it seems to be constrained to uplifted marine terraces, alluvial and colluvial deposits and paleosols (Claperton, 1993).

In Argentina, Late Cenozoic continental deposits mainly occur within the Chaco-pampean Plain, which extends from 20°S to 40°S at the Andean piedmont. These deposits form a wide sedimentary cover of variable thickness (up to a maximum of 300 m, Zárate and Orgeira, 2010). Pleistocene record is mainly composed of loessoid

* Corresponding author. Tel./fax: +51 11 4576 3329.
E-mail address: rtofalo@gl.fcen.uba.ar (O. Tófalo).

0895-9811/$ – see front matter © 2010 Elsevier Ltd. All rights reserved.
doi:10.1016/j.jsames.2010.09.001

sediments, modified by diagenetic pedogenic processes, which give rise to welded soils (Zárate, 2003).

So far, Stage 5 has been recorded at four sites (Kemp et al., 2006; Frechen et al., 2009) (Fig. 1). At both contributions, it is represented by paleosols, which have in turn been identified by luminiscense techniques. One of these sites is located near Baradero, in Buenos Aires province, where paleosols have developed on pallustrine sediments; they are gradually replaced by eolian sediments. A truncated paleosol developed on loess deposits and buried by fluvial sediments represents the Stage 5 at a profile located near Lozada, Cordoba province (Kemp et al., 2006). Frechen et al. (2009) reported loess/paleosols sequences from two sections at Monte Ralo and Corralito in Córdoba, Argentina. The luminescence dating study gives evidences for wet climate conditions with soil formation during the last interglacial period and early last glacial period correlating with Stages 5 and 3, respectively.

Zárate et al. (2009) report a pedosedimentary reconstruction at two sites (Hudson and Gorina) located in the northern Pampa of Buenos Aires Province. Their contribution also provides a detailed OSL chronology for both sites. Coastal marine sediments outcropping at Hudson (*ca.* 128 kyr) are correlated with MIS 5e. A paleosol developed on the marine deposits and the underlying paludal sediments. Its evolution and subsequent erosion took place between 128 and 54 Ka. At Gorina a pedocomplex was formed somewhere between 194 and 56 Ka.

A new record of MIS 5 is presented in this paper. It was found in a quarry placed near Zárate city, Buenos Aires province (34°09′S; 59°04′W) and it is represented by welded paleosols developed on loessic sediments (Fig. 1).

2. Environmental and geological setting

The Pampean region is a wide plain where Quaternary eolian sediments, partially reworked by action outcrop. It extends some 600,000 km^2 in the East-central region of Argentina (between 32–38°SL and 58–63°W). Landscape is rather plain to gently undulated.

The studied quarry is located in the "Pampa ondulada" ("Undulated Pampa"). This region is a narrow NW-SE belt extending between 32 y 35°S, in the southern portion of the Chacoparanaense Basin. Its relief is gently undulated and drained by small, ell defined creeks. At higher watersheds, Pleistocene loessic sediments belonging to the Buenos Aires Formation and occasionally to Ensenada Formation (Fig. 2). Recent and present-day fluviatile, eolian and palustrine sediments overlay those loessic horizons.

Topographic heights are moderate, range from 30 to 60 m high and increase northwestwards.

Landscape reflects eolian deflation and accumulation of loessic sediments during Late Cenozoic and Pleistocene recording comprises loessoid sediments deeply modified by pedogenic process giving rise to welded soils (Zárate, 2003).

According to Köppen (1923), the studied site belongs to the Pampa Húmeda and it is considered as being under a major climatologic type described as moist climates with mild winters (*Cfa: Humid Subtropical*).

The region is under the South Atlantic Anticyclone (SAA) influence that shifted north to south, producing changes in seasonal mean wind direction. During spring, a strong east component supplies moisture from the Río de la Plata meanwhile during the summer north–northeast winds, produce wet and warm air advection.

In winter when the SAA is located at its southernmost latitudinal position; the area is influenced by west and southwest winds and north–northeast winds.

Annual precipitation in the area is 1087.1 mm and the monthly mean temperature fluctuates between 10 and 23 °C.

3. Material and methods

The studied sequence can be considered as a sedimentary-pedological succession as described by Freytenet (1971). Discontinuities on sedimentation represented by erosion surfaces were identified and once they were established, units were defined regarding thickness, bed geometry, color, sedimentary and

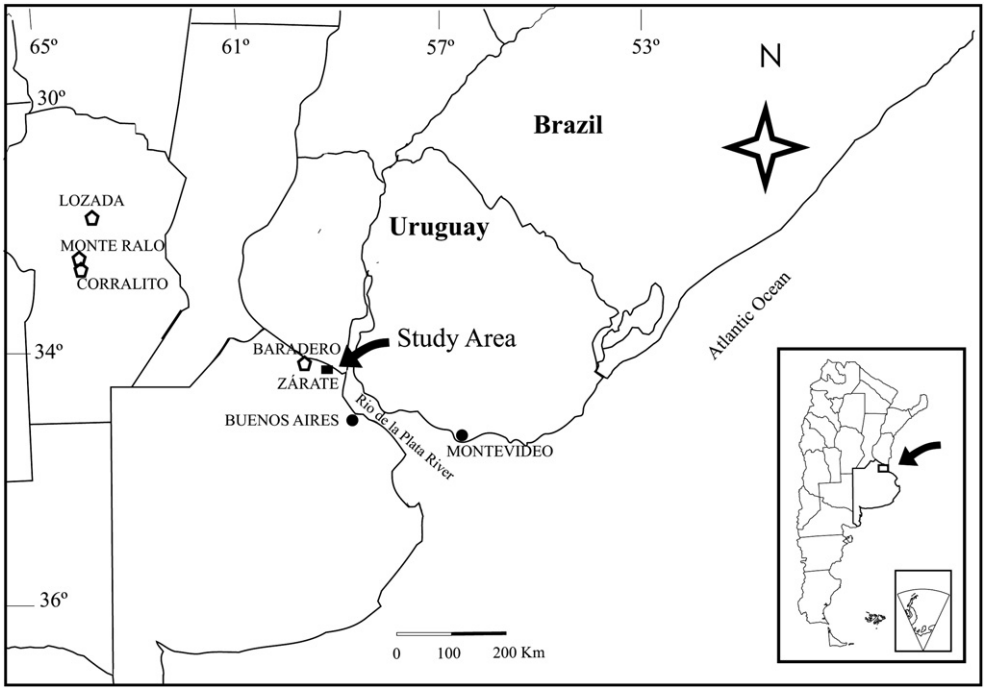

Fig. 1. Location map.

Ameghino (1880)	Riggi *et al.* (1986)	Valencio and Orgeira (1983)
Bonaerense	Buenos Aires Formation	Brunhes chron
Ensenadense	Ensenada Formation	Brunhes chron
		Matuyama chron

Fig. 2. Stratigraphic scheme and magnetic ages proposed for the "Pampa Ondulada" plain.

pedogenic structures, degree of consolidation, particle size parameters and composition. Color determination was made using the Rock Color Chart Committee chromatic standards. Lithofacies were defined after Miall (1996).

Preliminary paleomagnetic studies were carried out in order to set the magnetic age. The paleomagnetic sampling included the study of 11 stratigraphic levels distributed in lower section of the profile. The top of the profile did not sampled since the purpose of this paleomagnetic study was only to determine the position of the Brunhes/Matuyama transition.

Natural remanent magnetization was measured initially in all samples. They were analyzed to determine their magnetic stability. For this purpose, thermal demagnetizations were carried out in succesive stages between 100 and 400 °C, being increased step of 50 °C, and some samples up to 600 °C. Then, standard proceeding was then carried out to obtain the magnetic polarity (Valencio and Orgeira, 1983).

Samples taken at 1.2 and 7 m depth were sent to the Research Laboratory for Archeology and the History of Art, University of Oxford in order to determine their ages by optically stimulated luminescence (OSL) (Fig. 3). Ages were obtained on fine-grained quartz separations, using the single-aliquot regenerative-dose (SAR).

Representative samples were collected from every unit to perform particle size and mineralogical studies. X-ray diffraction analysis was carried out on oriented samples collected at 0.5 intervals or at points where conspicuous changes were observed. X-ray fluorescence analyses (Rb and Sr concentrations) were made on a closed-collected set of samples.

Particle size analysis was run on a CILAS 1180 particle analyzer. Histograms were built to determine location and type of modes. Percentiles used on calculation of Folk and Ward (1957) parameters were obtained from cumulative frequency curves plotted on probabilistic paper. Those curves also allowed to separate populations, which Visher (1969) assigned to tractive, saltation and suspension processes.

Samples were studied under petrographic microscope, regarding textural and compositional parameters. Paleosols were described after Bullock et al. (1985) and Stoops (2003). Carbonatic rocks were classified following Dunham (1962) and calcrete micro morphology was described after Wright (1990) who proposes two end members: alpha calcretes, which consists of a dense micritic or microsparitic groundmass in which floating, corroded and displaced grains and crystallaria are immersed and beta calcretes in which biogenic features such as rhizoconcretions, fibrous calcite, alveolar-septal textures, etc dominate. $CaCO_3$ contents were estimated optically.

Clay identification was performed by XRD, using a Phillips PW 1130 difractometer, Cu radiation, scan speed of 2°2Q per minute, at a range of 2×10^3.

Clay fraction was obtained by suspending sediments in distilled water and CALGON as a dispersing agent. Particles smaller than 2 μm were obtained by pipetting the suspension and aliquots were allowed to dry on three different glasses for each sample. One of them was analyzed after no other procedure. The other two were respectively treated under an ethylene glycol atmosphere for 24 h and calcination at 550° for 2 h.

Field number	Laboratory number	Age result number	Age estimate
Zárate-T1-CZ53	X630	OxL-1256	≥ 126,000 ± 10,000
Zárate-T2	X631	OxL-1257	30,000 ± 4,000

Fig. 3. Codes of samples analyzed by optically stimulated luminescence (OSL) and obtained results.

Once the species were identified, peak areas were measured and a semi quantification procedure was applied, by correcting areas using empiricfactors (Biscaye, 1965).

Rb and Sr concentrations were measured at INGEIS (Instituto de Geocronología y Geologçía Isotópica) by means of a Philips PW 1410 XRF spectrometer. Analyses were performed on whole rock samples powdered (fraction <200 mesh) and compacted. International standards GSP-1, AGV-1, NIST-1c and JLs-1 and were used as reference materials. Analytical uncertainties are ±2% for Rb and ±1.5% for Sr. These chemical determinations were carried out on 61 samples of the loessic sediments, paleosols and some calcareous levels which are intercalated in the sequence.

4. Results

The studied section, comprises a 10 m thick deposit. Eight meters of the section were studied in detail. According to their sedimentological features and magnetic ages, they are assigned to the Buenos Aires and Ensenada formations (Fig. 4).

Present day soil is found at the top of the section. Its parental material was sampled at 1.2 m where an OSL dating yielded an age of 30 ± 4 kyr. Another OSL age >126 ± 10 kyr for a sample taken at 7.3 m (non-pedogenic middle to upper part of the B unit) was obtained.

On the other hand, reverse polarity of the remanent magnetism suggests a Matuyama age (more than 0.7 Ma) for the bottom of the sequence, below paleosurface II. Overlying sediments show normal polarity of the remanent magnetism, so that a Bruhnes magnetic age is assigned (likely younger than 0.7 Ma). A small interval at the bottom of the sequence shows normal polarity, which could be a record of the Jaramillo event (0.91–0.98 Ma, Quidelleur and Valet, 1994).

Rb concentrations range from 78 to 99 ppm and Sr concentrations vary between 203 and 237, being the lower values always related to paleosols. Negative correlation between them is observed throughout the whole section. According to Dasch (1969), Chen et al. (1999, 2000), and Jin et al. (2005), the Rb/Sr ratio in paleosols is a good indicator of chemical weathering caused during pedogenic processes. The Rb/Sr ratio can be used to identify pedogenic levels within loess-paleosol sequences. Dissolved Sr is preferentially released to the weathering solutions. Carbonate minerals are removed and a relative enrichment in Rb contents occurs with the consequent increase in Rb/Sr ratio. The highest Rb/Sr ratios relates to the degree or intensity of pedogenesis. In this study, Rb/Sr values do not vary too much, but they still clearly increase in paleosol horizons (Fig. 4).

4.1. Unit A

Unit A, about 1.5 m thick, is tabular, with net base and top, both outlined by well-defined surfaces (I and II) (Fig. 4). The lower part comprises an unconsolidated very pale orange (10 YR 8/2) pelite. Pedogenic features are scarce at the bottom but they increase topwards, where pelites are moderately well consolidated and its color turns greyish orange pink (5 YR 7/2).

Histograms reflect unimodal distribution, with a main mode in coarse silt size and some important very fine psamitic and silty proximal admixtures (Fig. 5). Median and mean values are similar and indicate that the dominant grain size is coarse to medium silt. They are poorly to very poorly sorted, curves show very positive asymmetry and they are meso to slightly leptokurtic. Clay size fraction is less than 10%.

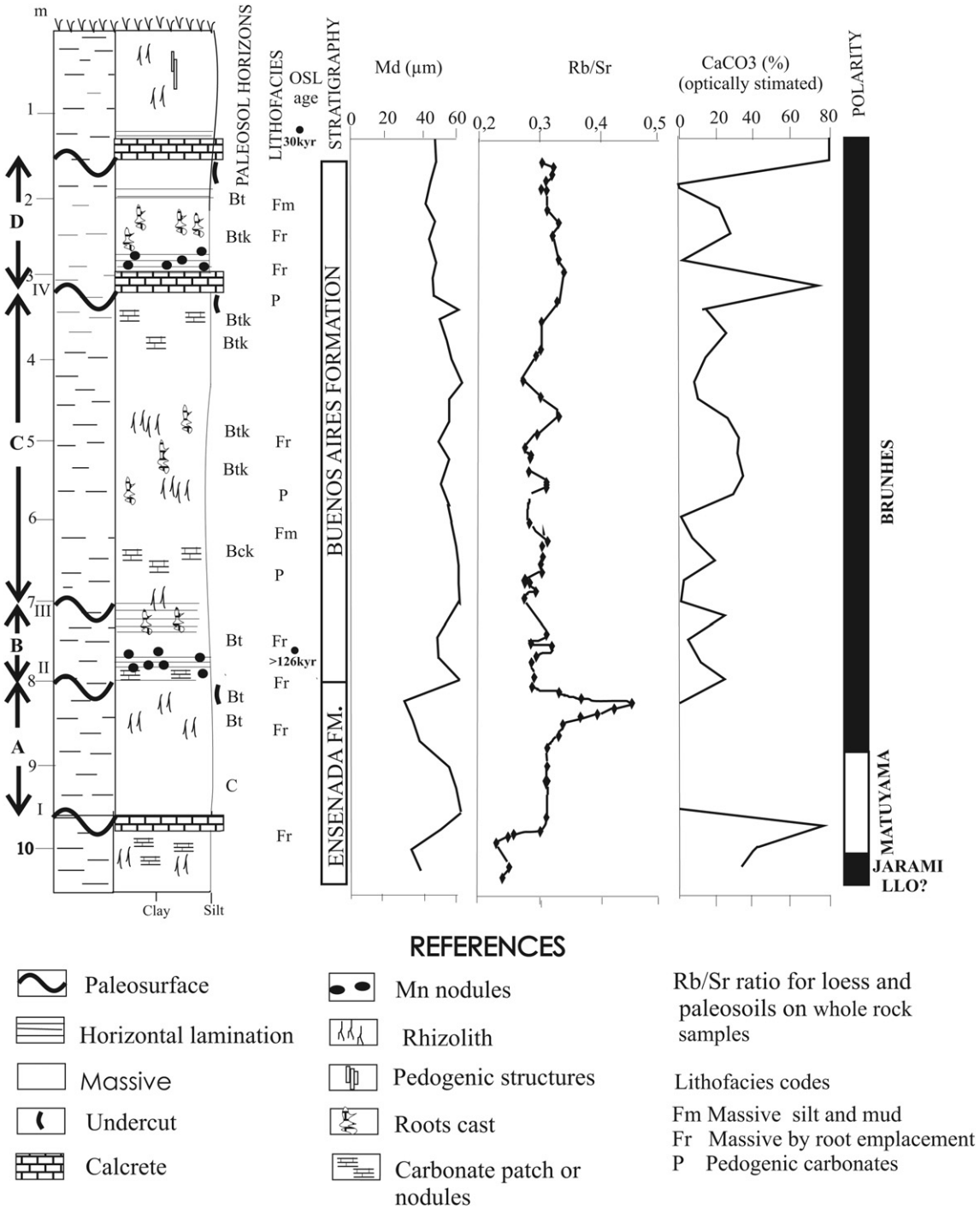

Fig. 4. Field log and depth functions of paleosol horizons, lithofacies, OSL ages, Md, Rb/Sr and % $CaCO_3$ from the profile at Zárate.

In the middle part of the section, sediments show a microstructure dominated by thin fissures with little separation of aggregates. Clast sizes range from silt to very fine sand with clay material among them. Pedofeatures include scarce aggregates of angulated blocks (Fig. 6). Pedality degree is weak. Peds are fine to medium, faces are serrated and unaccomodated. They are separated by zigzagging plain holes, with variable diameters. Channels are rare.

The ratio between skeleton and plasma materials following Stoops and Jongerius (1975) and using 4 μm as the limit value, the c/f ratio is 85/15. In case 30 μm is considered as the limit value, the c/f ratio changes into 50/50.

Groundmass shows dispersed speckled (Fig. 7a) or parallel striated b-fabric. Feldspar fragments (46%), volcanic ash (35%), quartz (15%), lithic volcanics (2%) and accessory minerals such as pyroxenes, amphiboles, opaque minerals and micas (2%) form the clastic fraction.

Textural pedofeatures are very fine grained discontinuous clay coatings (Fig. 7a), channel fillings formed by laminated clays, amiboidal or digitated orthic iron oxides nodules with undifferentiated internal fabric and moderate impregnation (Fig. 6).

The upper part of unit A sediments comprises of very fine and fine grained silt with clay among the clasts, which gives rise to

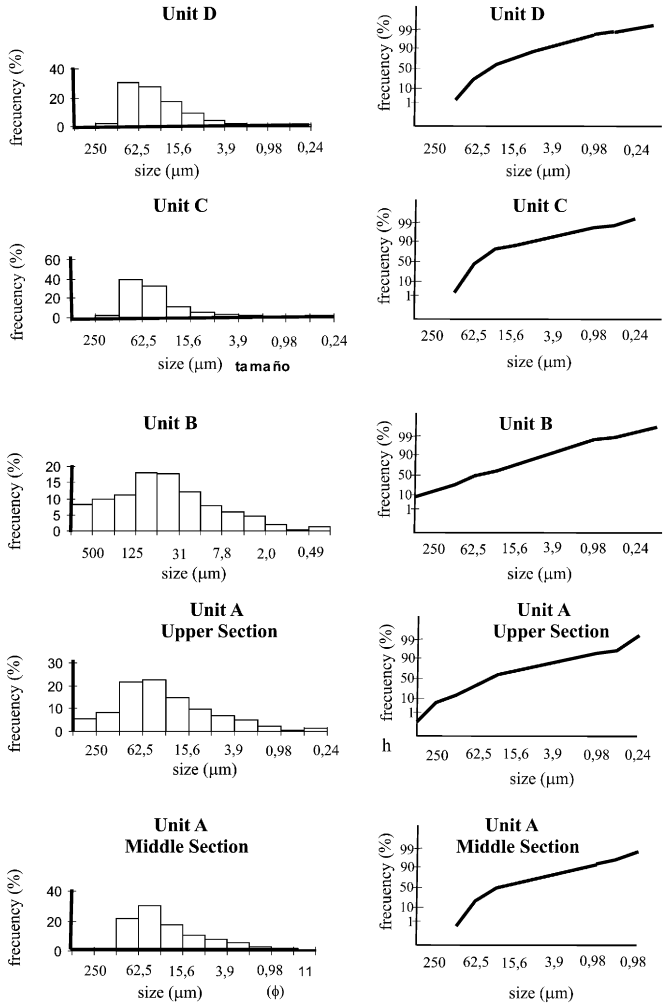

Fig. 5. Histograms and cumulative curves from representative samples.

a very tight packing. Pedality is weakly developed. Fine (50–100 μm) to medium (100–200 μm) meso channels showing generally unacommodated walls and mammilate surfaces, as well as medium (100–200 μm) to coarse (200–500 μm). All of them show clay coatings.

The ratio between skeleton and plasma materials senso Stoops and Jongerius (1975), using 4 μm as the limit value between them, is (c/f) 4 μm = 90/10. In case 30 μm is considered as the limit value, it changes into (c/f) 30 μm = 60/40.

The groundmass shows an undifferentiated fabric, and the clastic fraction comprises feldspar fragments (44%), volcanic glass (36%), quartz (15%), lithic volcanics (3%) and accessory minerals such as pyroxenes, amphiboles, opaque minerals and micas (2%).

Main pedofeatures are very fine grained discontinuous clay coatings and hypocoatings in the channels, minor amounts of iron coatings, amiboidal orthic iron oxide nodules with undifferentiated internal fabric, moderate impregnation and intercalated simple or serrate iron oxides (Fig. 6).

Only 10% of the sample corresponds to clay minerals. Illite is dominant and traces of an expandable mineral, probably vermiculite, are also present.

Deposits are massive and show pedogenic features, which allow to define them as Fr lithofacies (massive, bioturbated, root-bearing silts and clays).

The features of Unit A point out loessic sediments deposited by winds on gentle slopes.

The mineralogical composition of sand and coarse silt fractions indicates an unequivocal volcano-pyroclastic provenance. Illite clearly dominates the basal section of the unit. Scarcity of pedofeatures at this level supports a detrital origin for this clay. On the other hand, middle and upper part of the unit, show pedofeatures, such as speckled or parallel striated b-fabric, fine and medium blocky structures as well as different types of coatings and iron oxides nodules due to illuviation.

Illuvial concentration of clay is also recorded by the strong positive asymmetry of cumulative curves (fine tails). Bioturbation was probably active and is evidenced by the amount and diversity of channels.

On this basis the lower section of this unit is interpreted as a C horizon while middle and upper parts are proposed to be a Bt horizon.

4.2. Unit B

Unit B is 1 m thick, base and top are net and they are bounded by paleosurfaces (II and III). It is moderate orange pink in color (5 YR 8/4) and its geometry is tabular. Manganese nodules as well as calcium carbonate concretions are present. In the lower part, calcium carbonate laterally forms a massive calcrete, irregular in thickness and grayish orange pink (5 YR 7/2). Above this calcrete, an undulate laminar structure occurs, due to subhorizontal calcite infilled-vesicles. Laminaes are 1–2 cm thick, and they appear irregular and discontinuous. Carbonate distribution results in consolidation of this part of the unit, while the middle part remains unconsolidated (Fig. 4).

Pedofeatures are scarce throughout the middle part of this unit, but they become relevant towards the upper part where vertical root casts and calcium carbonate nodules occur. The top is outlined by abundant subhorizontal vesicles, sometimes infilled by calcium carbonate.

These sediments are unimodal, with a poorly defined mode in very fine sand (18.1%) slightly higher than the important (17.7%) coarse silt sized proximal fine admixture (Fig. 5). Median and mean values are similar and indicate that the dominant grain size is coarse silt. Sediments are very poorly sorted, thus the curves are mesokurtic and simmetric. The segment of the cumulative curve representing sand and coarse silt size populations is better developed (65%) than that corresponding to finer grains is shorter (35%). Clay size fraction is about 9.5% of the deposit.

Sediments forming the lower part of this unit are calcretes, in which authigenic micritic carbonate, splits and continuously cements 15% corroded monomineralic grains and loessic fragments. The massive part is a dense, alpha-type calcrete (Fig. 7b) petrographically classified as wackestone. Fractures and crystallaria are common together with some partially filled chambers. Crumb texture, due to recrystallization into microsparite is observed. Internally, in the laminar structure, some laminae consist of micrite forming concentric coatings surrounding a pore, other contain etched detrital grains within micrite, with common alveolar-septal structure (Fig. 7c).

Sediments from the upper section of unit B are very porous. The microstructure is dominated by subangular mamillate fine (5–10 mm) to very fine (<5 mm) blocks (Fig. 6). Pedality is strongly developed.

Aggregates are separated by fine (50–100 μm) to medium (100–200 μm) mesopores (less than 15%), with accommodated faces. Pores are zigzaging or vermiform planar voids, mostly infilled by calcite. Fragmented clay coatings embedded within groundmass are observed (Fig. 7d).

Skeleton/groundmass ratio, using c/f after Stoops and Jongerius (1975), is c/f at 4 μm = 90/10 In case 30 μm is considered as the limit

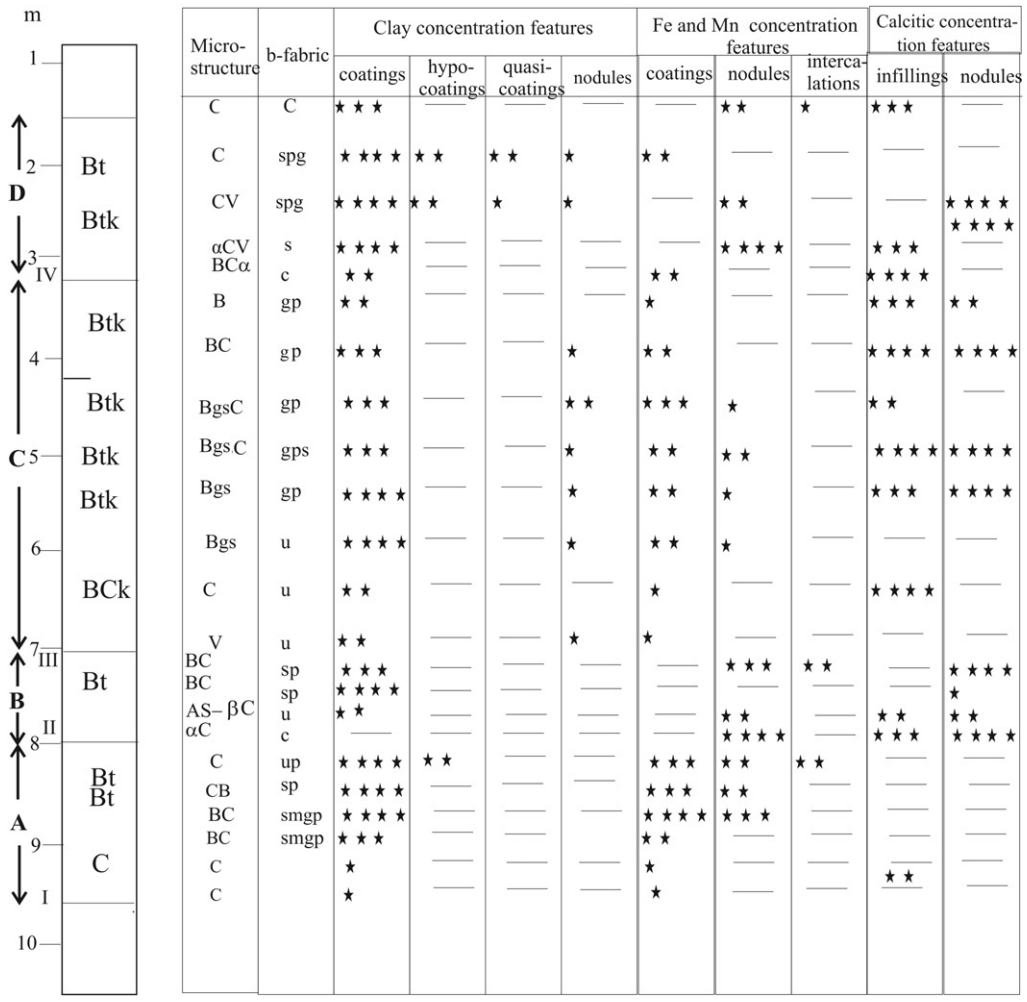

Microstructure

α Alpha fabric

AS Alveolar Septal Structure

β Beta fabric

B Blocky

Bc Breccia calcrete

Bgs Bridged grain structure (gefuric)

C Channel

V Vughy

B- fabric

c Cristallitic

g Granostriated

m Parallel striated

p Porostriated

s Speckled

u Undifferenciated

—— Not detected

★ rare (< 0,5%)

★★ Very few (0,5 - 3%)

★★★ Few (3 - 5%)

★★★★ Common (> 5%)

Fig. 6. Micromorphological features of the profile at Zárate.

value, it changes into (c/f) 30 μm = 65/35. Some sectors of the groundmass show a very poorly defined speckled fabric.

The coarse fraction comprises feldspar grains (47%), volcanic glass fragments (34%), quartz (15%), lithic volcanic fragments (2%) and accessory minerals such as pyroxenes, amphiboles, opaque and micas (2%).

Most relevant textural pedofeatures are planar clay coatings and laminar clays infilling channels (Fig. 6). Most of the pores are filled by sparitic calcite, sometimes as rhombic crystals which outlines peds limits. Scarce amiboidal orthic iron oxides nodules are present. Impregnation is mostly moderate, although it is strong at some small nodules.

Only 10% of these sediments are clay sized. The clay assemblage sampled in the upper part of this unit is illite dominated (85%), and a subordinate (15%) expandable phase, probably vermiculite is also present.

The lower part of the unit is a discontinuous calcrete while the upper portion, comprises pelitic and a very fine sand material with strongly developed pedality, so that Fr lithofacies is assigned (silts and clays with roots and bioturbation).

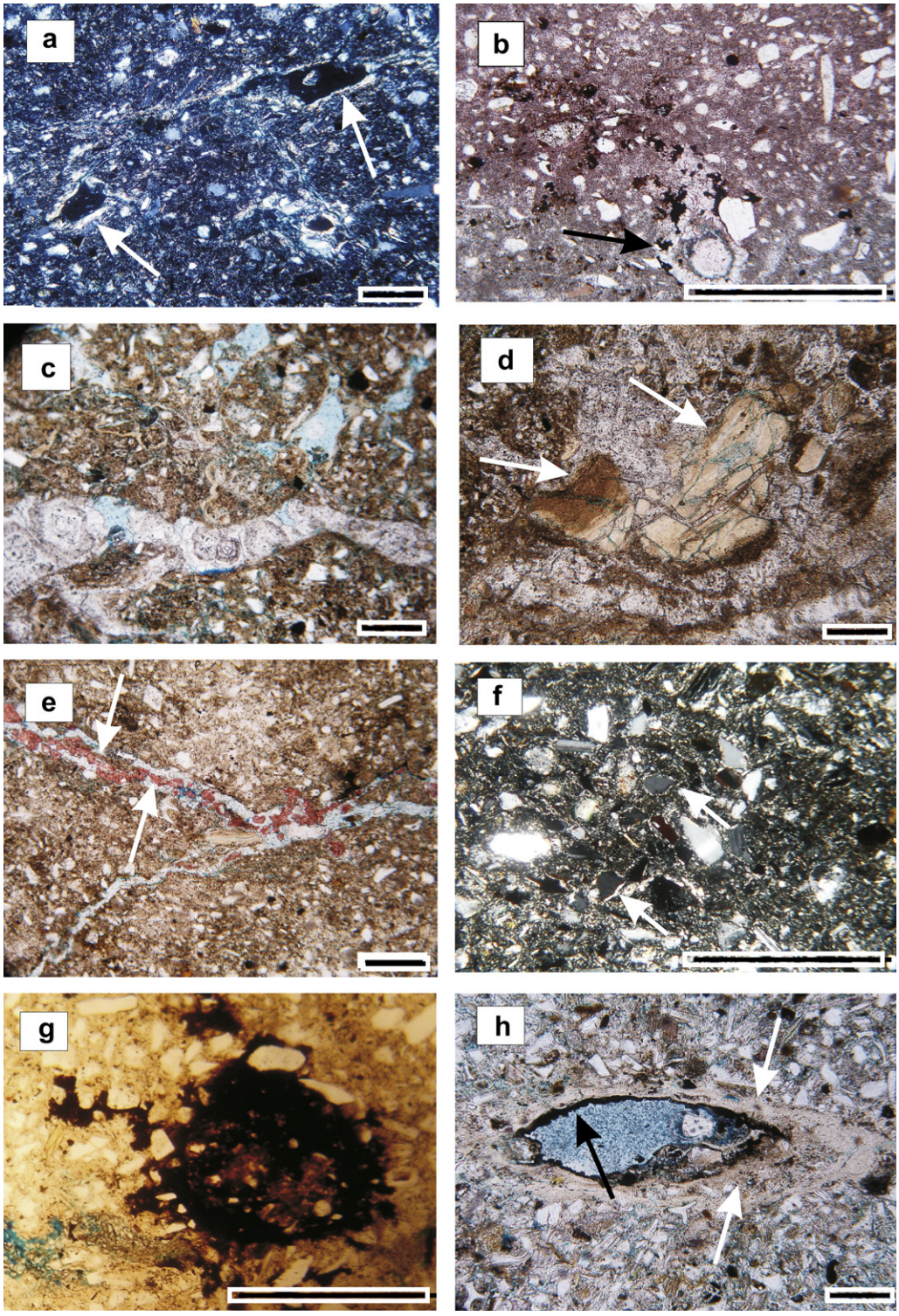

Fig. 7. Photomocrographs of key micomorphological features: plane polarized light (PPL), crossed polarized light (XPL); scale bar = 500 μm. a) dispersed speckled b-fabric and clay coatings around channels (white arrows). b) alpha fabric or cristallitic b-fabric with calcitic hypocoatings (black arrow) (PPL). c) alveolar-septal structure (PPL). d) fragmented clay coatings (white arrows) embedded within groundmass (PPL). e) calcitic hypocoatings around fissures (PPL). f) stipple speckled b-fabric, and clay coatings (white arrows) around grains (XPL). g) ferric nodule embedded within groundmass (PPL). h) ferric coating (black arrow) covering (postdating) a clay coating (white arrows) around a channel (PPL).

The features of Unit B also indicate a loessic origin. The massive discontinuous calcrete, well indurated in comparison with the host material, indicates strong cementation by shallow ground waters. Evidences are alpha fabric (complex fractures, crystallaria, floating corroded grains, and dense fabric) which occur as a result of dispalcive growth of calcite within the hosting sediment, indicate that the calcrete has formed mainly due to evaporation, evapotranspiration, and gases loss (Wright and Tucker, 1991).

This calcrete is covered by an undulated laminar calcite structure, which is related to horizontal roots (Wright et al., 1995). Evidences are the morphology of the laminaes, with a central pore and a coating of micrite, interpreted like cortex root calcification

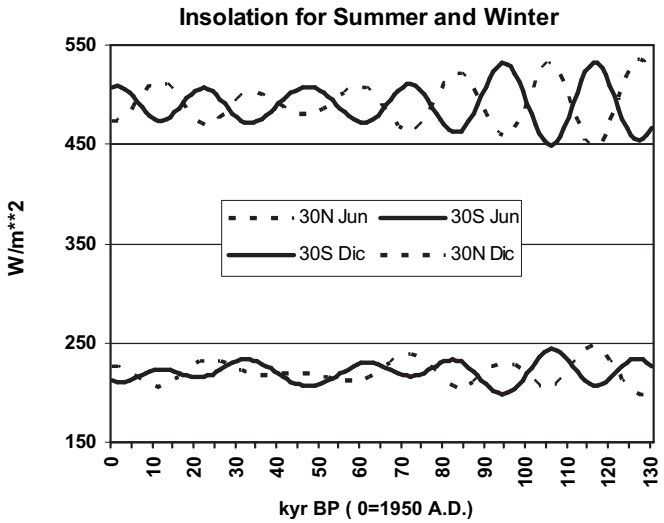

Fig. 8. Insolation for summer and winter.

(Alonso Zarza, 1999), and the alveolar-septal structure, characteristic of β-fabric.

The laminae must have formed within the soil where plants were forming a root mat. The carbonate growth breaks, displaces and replaces the host material, as well as it etches the detrital grains. Different plants may form horizontal laminae or root mats. Their formation is controlled by the supply of water (Alonso Zarza, 1999), either from shallow water tables (Mack and James, 1992) or vadose water retained within the sediment.

The formation of root matswithin detrital sediments or soils indicates relatively short periods of no sedimentation and stabilization, in which the laminae developed, followed by rapid periods of sediment accumulation, erosion or high sedimentation rates that inhibit both laminae formation and preservation (Alonso Zarza, 1999).

The micro morphology of both types of calcretes points to a vadose and phreatic environment. Micrite reflects a rapid precipitation at vadose zone, from supersaturated solutions, which destroys and displace primary fabric.

Secondary microsparite occurs as a replace of the original micritic mud due to dissolution and re-precipitation processes (Tandon and Narayan, 1981). Crystallaria may have originated as a result of dissecation, expansive growth and infilling of roots casts. Manganese nodules may be related to pH increasing because of calcium carbonate presence, which catalyzes oxidation of Mn^{2+} turning it into MnO_2. Their presence indicates changes in Eh related to periodical water saturation stages.

The upper part of the unit is a paleosol with strongly developed pedality, and speckled b-fabric. Parental material is volcano-pyroclastic, although it is now strongly modified. Illuviation of clay minerals from upper levels is recorded by clay coatings. This portion of Unit B is thus interpreted as a Bt horizon. However, the fractured clay coatings suggest a more complex pedosedimentary history, perhaps a polycyclical story of deposition, pedogenesis and re-working.

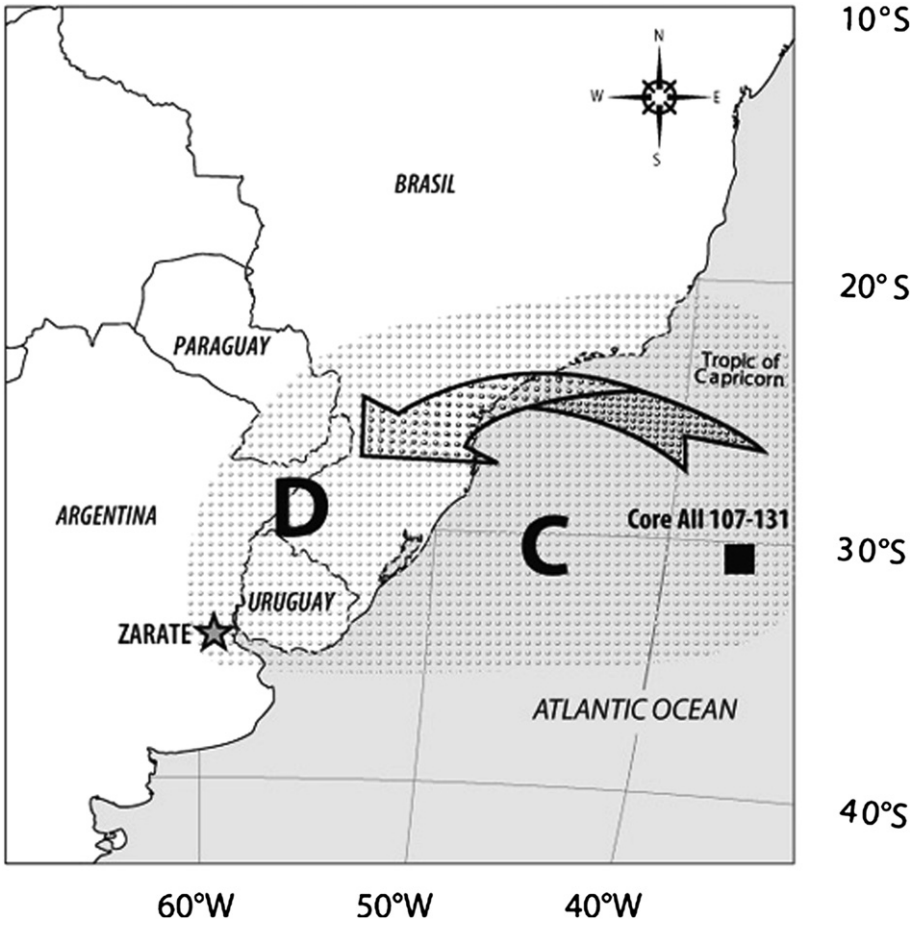

Fig. 9. Large scale wind convection pattern during Austral spring, summer, and fall.

Illite is inherited from loessic material, while vermiculite is pedogenic. Sparitic calcite infilling channels are lately precipitated from phreatic water. It is indicated by its interstitial occurrence as well as the shape and size of crystals.

4.3. Unit C

This unit, 3.75 m thick, is tabular, with net base and top, both of them are outlined by well-defined undercuts (III and IV). The color is grayish orange (10 YR 7/4) and it turns paler at the outer sectors (very pale orange 10 YR 8/2), due to the presence of calcium carbonate (Fig. 4). It is moderately consolidated and highly porous. Abundant subhorizontal vesicles are found at the base. The lower section is massive but middle and upper ones are characterized by the occurrence of rhizolites, pedofeatures and carbonate patches. Rhizolites are mostly root casts, after Klappa (1980), as a result of calcite infilling of root moulds.

These sediments are unimodal, with a main mode in very fine sand size (39.3%) slightly higher than the important coarse silt sized proximal admixture (32.7%) (Fig. 5). Median and mean values are similar and indicate that the dominant grain size is coarse silt. They are very poorly sorted, curves show very positive asymmetry and they are leptokurtic. The segment of the cumulative curve representing saltation moving – sand and coarse silt size populations is the best developed (75%), while the portion characterizing finer grains is smaller 25%. Clay size fraction forms only 5.28% of the deposit.

The sediments of the middle part of the unit are very porous and apedal. Bridged grain (gefuric) microstructure is observed, with sand and silt grains mostly coated by fine material forming bridges and meniscus among grains. Aggregation is scarce, mainly due to some degree of discontinuity of coatings. Few elongated and randomly distributed middle sized meso channels (100–200 μm) occur (Fig. 6). They have curved walls and are partially infilled by clay and ferruginous coatings.

The upper part of Unit C shows microstructure dominated by thin fissures with little separation of angulated blocks. Calcite hypocoatings fill the fissures (Fig. 7e). Groundmass shows dispersed speckled b-fabric and clay coatings around grains and pores are common (Figs. 6 and 7f).

Skeleton/groundmass ratio is c/f at 4 μm = 94/6. In case 30 μm is considered as the limit value, it changes into (c/f) 30 μm = 75/25. The coarse fraction comprises volcanic glass fragments including both ash and pumice (51%), feldspar grains (31%), quartz (12%), lithic volcanic and shale fragments (3%) and accessory (mainly opaque) minerals (3%).

Most relevant textural pedofeatures are clay coatings, iron hypocoatings, calcitic nodules and seldom clayey aggregate-like orthic nodules with undifferentiated internal fabric (Fig. 6).

Five XRD analyses were performed for this unit. The lower section assemblage has dominant illitic material (about 70%) and low cristallinity smectite. The middle section presents an illite dominated (90%) assemblage, bearing little (10%) vermiculitic material followed upwards by another illite dominated assemblage (80%) with 20% of smectite. To the top, illite amount decreases to 60% while smectite makes up to 40% of the clay minerals.

Fm is found at the lower part of this unit, while grain size and pedofeatures of the middle and upper parts of the unit stand for an Fr lithofacies assignment (massive, root-bearing, bioturbated silts and clays).

The shape of the deposits, lack of primary structures and textural characteristics of Unit C again suggest a loessic origin for this unit. Provenance is also volcano-pyroclastic. This unit is strongly affected by pedofeatures, which become more significant towards the middle and upper sections. The lower part, with little macroscopic evidences of pedality and high amounts of calcium carbonate, could be related to a BCk horizon. The middle section shows a bridged grain microstructure (gefuric), and diverse types of coatings indicating illuviation from upper levels.

The upper section with blocky microstructure, dispersed speckled b-fabric and clay and calcitic coatings also point out the presence of paleosoil horizons. Root casts and carbonate patches indicate that they are pedality Btk horizons. Thickness of the unit together with the repetitive superposition of these features supports the occurrence of several welded horizons. Fluctuation of clay mineralogy is also standing for welding. Illite dominance restricted to A horizons and smectite enrichment in Bt and BC horizons has been reported in nearby soils (Orgeira et al., 2008).

4.4. Unit D

Unit D is about 1.5 m thick, with slightly undulated net base and top, both outlined by well-defined surfaces (VI and V) and undercuts. It is tabular, appears as moderately well consolidated and its color is very pale orange (10 YR 8/2). An irregular calcrete locates at the base. Its upper part shows a typical undulated laminar structure due to the penetration of calcium carbonate into the vesicles of hosting sediments. Manganese nodules are common and vertical rhizolithes are frequently observed at the middle sector. Pedofeatures are abundant. Few irregular lenses 15–20 cm thick and 2 m long occur laterally. They are formed by pale olive (10 YR 6/2) clays.

These sediments are unimodal, with a main mode in very fine sand size (30.4%) slightly higher than the important coarse silt sized proximal admixture (27.6%). On the other hand, the coarse proximal admixture, corresponding to fine sand is very scarce (2.5%) (Fig. 5).

Median and mean values are similar and indicate that the dominant grain size is coarse silt. They are very poorly sorted, and curves are leptokurtic and show very positive asymmetry. The segment of the cumulative curve representing saltation moving – sand and coarse silt sized populations is the best developed (60%), while the portion characterizing finer grains is shorter (40%). Only 4.6% of the deposit is clay sized.

The lower section of this unit is formed by a brecciated calcrete. Sparitic carbonate with mosaic texture cuts, separates and cements shale and argillite fragments, displaying a two directions-pattern.

An α-fabric is sometimes developed as a result of concentration of micritic carbonate. It is a dense microfabric, due to displacive growth of micrite. Some channels occur, because of holes left by roots. They are coated by laminar clay coatings and infilled by granular sparite. Some of them show iron oxides hypo and quasi-coatings. Irregular and circumgranular crystallaria are common as well as iron oxide aggregates. Petrographic classification for this sedimentite is wackestone.

The middle and upper sections of this unit are apedal. Microstructure shows few coarse meso channels (200–500 μm), and medium (1–2 mm) to fine (500–1000 μm) macro channels and vuggy structure. Cavities have smooth curve walls. Pores are unoriented and randomly distributed, sometimes coated by laminated clay coatings and iron coatings.

Skeleton/groundmass ratio is c/f at 4 μm = 92/8. In case 30 μm is considered as the limit value, it changes into (c/f) 30 μm = 60/40. Groundmass shows a poorly defined speckled fabric. Coarse fraction comprises feldspar grains (47%), volcanic glass fragments (40%), quartz (10%), lithic volcanic fragments (1%) and accessory minerals such as pyroxenes, amphiboles, opaque minerals and micas (2%).

Most relevant textural pedofeatures (Fig. 6) are iron oxide orthic nodules (Fig. 7g) and intercalations with moderate to strong impregnation, clay coatings, laminated iron hypo and quasi-coatings in cavities and channels (Fig. 7h), and scarce clay nodules.

Clay minerals are scarce (8%), and the assemblage is illite dominated (55–60%), with an important amount of regular to high crystallinity smectite (40–45%).

The basal section of this unit is a calcrete. Middle and upper part can be described as an Fr lithofacies (silts and pelites with roots and bioturbation).

The tabular shape, lack of primary sedimentary structures and textural features of Unit D also suggest a loessic genesis for this unit. Sand and silt sized components are of volcano-pyroclastic origin. Macro and microscopic features of the irregular brecciated calcrete at the bottom of the unit, including fractures and channels due to roots (some of them with illuvial characteristics), suggest a pedogenic origin.

The upper sector, with undulose laminated structure is a typical feature of laminar calcretes formed by horizontal roots (Alonso Zarza, 1999).

Brecciation characterizes vadose diagenetic environment, where cementation and non-tectonic fracturing conditions alternate repeatedly. Origin of fractures affecting the hosting material may be due to dissecation phenomena, root action – related pores and displacement provoked by calcite growth. Cleaved primary sparitic calcite crystallaria infilling fractures, precipitate from highly supersaturated solutions in diagenetic phreatic environment. As explaind before, manganese nodules could have formed by pH increasing, due to calcium carbonate which catalyzes Mn^{2+} oxidation giving rise to MnO_2. Their presence indicates changes in Eh related to periodical water saturation stages.

Middle and upper sections show apedal soil horizons. The microstructure is dominated by channels and cavities indicated bioturbation processes. Several types of clay coatings and iron oxide nodules are observed, indicating illuviation processes from upper horizons.

Dominance of illite over smectite outlines the importance of argilo-illuviation processes from upper levels. Abundance of root casts in vertical position in the middle section, possibly indicates a Btk horizon.

The upper section without calcium carbonate concentration should be considered a Bt horizon.

5. Discussion

Four Late Cenozoic continental sedimentary sub-cycles have been recognized within the Pampean region deposits (Zárate, 2003; Zárate and Orgeira, in press). The pedosedimentary section studied in this paper can be related to the last part of the third subcycle (circa 3.2 Ma/0.040–0.030 Ma), which comprises Marplatense, Ensenadense and Bonaerense stages-ages.

Kemp et al. (2006) recently analyzed some sections outcropping within northern Pampean region (Baradero in Buenos Aires and Lozano in Córdoba), and performed some OSL datings on those deposits. Upon this basis, a paleosol, identified at both sections, was assigned to the MIS 5.

The section here presented is cyclic and complex. It comprises deeply pedogenetically modified loessic deposits, and shows several hiatuses outlined by discontinuities.

Paleosols are well developed throughout the whole section, indicating non-sedimentation and pedogenic dominance periods, probably interrupted by periodical erosion that removed the superficial horizons. It is evidenced by paleosurfaces. New loessic accumulations and pedogenesis took cyclically place. The apparent lack of A horizons could be a result of erosion due to climate shifting to drier conditions which would have originated paleosurfaces. On the other hand, these horizons may have become unrecognizable by pedogenetic processes (Zárate et al., 2002). Frequent evidences of bioturbation indicate that these process were effectively active while sediments were being deposited, leading to changing A horizons into B or C ones. Some degree of re-working is suggested by the occurrence of fragmented clay coatings.

A brief comment should be made on Paleosurface II as its significant magnitude, which generates a several thousand years gap, could be the result of neotectonic events. Several authors have proposed this kind of events for the central region of Argentina from Late Pleistocene up the present (Costa and Vita-Finzi, 1996; Costa et al., 1999, 2001; Brunetto and Iriondo, 2007). One or more than one of these episodes could stand for the uplift resulting in the erosion recorded by this surface.

Parental material though strongly modified is recognized as volcano-pyroclastic for all the units. Presence of calcretes indicates periods or areas with little clastic supply, strong climatic control and conspicuously seasonal arid or semiarid climate (Alonso Zarza, 2003).

Only the massive calcrete observed at the bottom of Unit B seems to reflect vertical and lateral change in water table. This is supported by strong cementation and the presence of alpha fabric. Calcretes found within units B, C and D, are pedogenetic, regarding the presence of undulose laminated structure or root mats, vertical root casts, alveolar-septal structure, indicating development in well-drained soils.

Calcium carbonate accumulation in B horizons, which leads to the formation of calcretes, is the most relevant pedogenetic process in dry subtropical zones (Mack and James, 1994). Annual rainfall rate is less than 1000 mm and seasonality is conspicuous.

Iron oxides, smectites and illite-bearing pedogenetic calcretes, as Units C and D, indicate semiarid climates, with annual rain rates between 100 and 500 mm (Khadkikar et al., 2000).

No calcretes of any origin are found at present soils (Argiudols when well-drained and Natracuols when poorly drained). These soils have developed under subtropical humid climate. Climatologic data suggest water excess almost around the whole year (Orgeira et al., 2008).

Fig. 4 summarizes the sequence of pedosedimentary stages responsible of the Zárate succession. Unit A involved a period of loess sedimentation followed by establishment of land surface and development of a soil with blocky structures, important clay and iron illuviation and active bioturbation. A Matuyama magnetic age (more than 0.7 Ma) is estimated for this unit, while a Brunhes age (less than 0.7 Ma) is suggested for the upper pedosedimentary units.

After an unconformity, Unit B was developed. It started as a period of loess sedimentation followed by surface stabilization, and the generation of a groundwater calcrete, representing an impermeable horizon above which root mats were developed. At the top, a soil with speckled b-fabric was formed and clay translocation became a prevalent processes.

After another discontinuity a similar sequence of events was developed. However, the pedosedimentary history was more complex, resulting in alternating loess deposits and several welded paleosols, with bridged grain and blocky microstructures, root casts and clay translocation processes.

The OSL age of >126 kyr obtained for upper middle part of Unit B, suggest that this unit as well as unit C, could have been developed to the end of the latest interglacial stage, which is equivalent to the isotopic Stage 5 found at marine deposits. Taking into account that OSL age could give a minimum age, it could be possible that this pedocomplex represents an older climatic warming.

Loess kept accumulating, so generating Unit D. When the land surface was stabilized a new pedogenic calcrete developed at the bottom and a soil at the top, with microstructure dominated by channels indicating active bioturbation and prevailing illuviation processes. Although further precision should be achieved for unit D its sediments could represent MIS 4 while pedogenic levels developed on them, would record MIS 3 or an older warm period.

Finally, deposits found at the top of the sequence could be temporarily related to MIS 2 or an older glacial one.

The studied sequence, according to paleomagnetic data, can be correlated to the middle and upper sections of the Baradero section studied by Nabel et al. (2000). The Paleosurface II (this study) could correspond to the El Tala geosol of these authors meanwhile the lowest 2.5 m of the here-studied deposit could be assigned to the Ensenada Formation.

6. Paleoclimatic assessment

The last interglacial stage, corresponding to MIS 5, extends from 127 kyr to 118 kyr (Siddall et al., 2007).

These changes in orbital conditions found a different insolation behavior response in the Southern Hemisphere, as reported by Winter et al. (2003). Fig. 8 shows insolation values for 30°S latitude, a position which is similar to that of localities studied in Argentina. Higher variations of insolation can be observed for the summer time (mid-month December).

During MIS 5 summer time average insolation was lower than that for Holocene times in the Southern Hemisphere. In December, it was ~491.6 W/m^2 between 125 kyr and 106 kyr BP. (~500.57 W/m^2 from 125 kyr to 126 kyr BP). During the Holocene (10 kyr BP to present) it was ~502.16 W/m^2 in average. The present value is 507.27 W/m^2.

The opposite situation took place in winter (June). During MIS 5, average values were ~218 W/m^2 from 125 kyr to 116 kyr BP (~223.29 W/m^2 from 125 kyr to 126 kyr BP), higher than those recorded during Holocene (~214.28 W/m^2). According to the correlation suggested in this contribution, summer time conditions for MIS 5 were colder than those recognized for the Holocene.

Although a detailed paleoclimatic assessment needs to be supported by well chronologically calibrated data, some general considerations can be proposed for the studied section at Zárate. The available data suggest that climate during MIS 5 was drier than it was during the Holocene. From a strictly climatological point of view, this could be related to lower temperatures during the summer.

In the present time, in South America, a large scale convection system starts in the Austral spring and the rainy season persists until fall. According to Doyle and Barros (2002), a regional maximum in precipitation field centers at about 30°S and 55°W, within the path of the main stream of the low-level moisture transport. Furthermore, the sea surface temperature (SST) in the Eastern subtropical South Atlantic Ocean is directly related to the precipitation in subtropical South America. The SST is tightly related to evaporation, so that warm anomalies imply higher humidity in the air mass arriving at the studied area.

Zárate is located within this region, where humidity rates of the air mass strongly force precipitations intensity.

On the other hand, core All07-131 at 31°S and 38°W (Imbrie et al., 1992; Boyle, 1984) is located at the centre of the Eastern Subtropical South Altantic Ocean, so that a warm (cool) SST could lead to a wet (dry) period in the Zárate region (Fig. 9).

The $\delta^{18}O$ proxy from the core is higher for MIS 5e (mean. 2.895 and s.d.: 0.120) than in the Holocene (mean 2.775 and s: 0.256). Therefore, the SSTs were low during MIS 5 probably leading to lower evaporation rates than those occurring in the Holocene.

7. Conclusions

- The studied section located within the Pampa Ondulada is an important Late Quaternary record for the southern hemisphere at medium latitudes.
- It comprises loessic sediments with strong pedogenesis, thus forming a complex cyclic sedimentary-pedogenetic sequence. In spite of discontinuities due to several erosion surfaces, these units should be studied at a higher resolution.
- Unit C bears welded paleososls probably related to MIS 5. These paleosols could be correlated with those developed at Lozada (Córdoba, Argentina) and Baradero (Buenos Aires, Argentina), studied by Kemp et al. (2006) and Corralito and Monte Ralo (Córdoba, Argentina) studied by Frechen et al. (2009).
- Pedogenic calcretes and horizons showing clay translocation provide very interesting information about climate, which seems to have been drier than present and strongly seasonal. The formation of root mats indicates relatively short periods of no sedimentation and stabilization followed by rapid events of sedimentation.
- According to the suggested interpretation, the geological record at Zárate could indicate that climate during MIS 5 was drier than it was during the Holocene. From a strictly climatological point of view, this could be related to lower temperatures during the summer.

Acknowledgements

The authors are grateful to the Universidad de Buenos Aires (Argentina) for their institutional support. This work was carried out under UBACyT grant X236, X219 and X445 and PICT 00438, PICT 0382/07, PIP 747/10, which provided financial support for the research.

References

Alonso Zarza, A., 1999. Inicial stages of laminar calcrete formation by roots: examples from the neogene of central Spain. Sedimentary Geology 126, 177–191.

Alonso Zarza, A., 2003. Palaeoenvironmental significance of palustrine carbonates and calcretes in the geological record. Earth-Science Reviews 60, 261–298.

Biscaye, P.E., 1965. Mineralogy and sedimentation of recent deep-sea clays in the Atlantic Ocean and adjacent seas and oceans. Geological Society of America Bulletin 76, 803–832.

Boyle, E.A., 1984. Sampling statistic limitations on benthic foraminifera chemical and isotopic data. Marine Geology 58, 213–224.

Brunetto, E., Iriondo, M.H., 2007. Neotectónica en la Pampa Norte (Argentina). Revista de la Sociedad Geológica de España 20 (1–2), 17–29.

Bullock, P., Federoff, N., Jongerius, A., Stoops, G., Tursina, T., Babel, U., 1985. Handbook for Soil Thin Section Description. Waine Research Publications, England, 150 pp.

Claperton, C., 1993. Quaternary Geology and Geomorphology of South America. Elsevier, 769 pp.

Chapman, M.R., Shackleton, N.J., 1998. Millenial-scale fluctuation in North Athantic heat flux during the last 150,000 yrs. Earth and Planetary Science Letters 159, 57–70.

Chen, J., An, Z., Head, J., 1999. Variation of Rb/Sr ratios in the loess-paleosol sequences of Central China during the last 130,000 years and their implications for monsoon paleoclimatology. Quaternary Research 51, 215–219.

Chen, J., Wang, Y., Chen, Y., Liu, L., Ji, J., Lu, H., 2000. Rb and Sr geochemical characterization of the Chinese loess stratigraphy and its implications for palaeomonsoon climate. Acta Geologica Sinica – Journal of the Geological Society of China 74 (2), 279–288.

Costa, C.H., Vita-Finzi, C., 1996. Late Holocene faulting in the southeast Sierras Pampeanas of Argentina. Geology 24, 1127–1130.

Costa, C.H., Giaccardi, A.D., González Díaz, E., 1999. Paleolandsurfaces and Neotectonic Analysis in the Southern Sierras Pampeanas, Argentina. In: Geological Society, London, Special Publications, vol. 162, pp. 229–238.

Costa, C.H., Murillo, M.V., Sagripanti, G.L., Gardini, C.E., 2001. Quaternary intraplate deformation in the Southeastern Sierras Pampeanas, Argentina. Journal of Seismology 5, 399–409.

Dasch, E.J., 1969. Strontium isotopes in weathering profiles, deep-sea sediments, and sedimentary rocks. Geochimica et Cosmochimica Acta 33, 1521–1552.

Doyle, M.E., Barros, V., 2002. Midsummer low-level circulation in subtropical South America and related precipitation patterns. Journal of Climate 15, 3394–3410.

Dunham, R.J., 1962. Classification of carbonate rocks according to depositional textures. In: Han, W.E. (Ed.), Classification of Carbonate Rocks. American Association Petroleum Geologists Memoir vol. 1, 108–121. Tulsa.

Folk, R.L., Ward, W.C., 1957. Brazos river bar: a study in the significance of grain size parameters. Journal of Sedimentary Petrology 37 (2), 514–521.
Frechen, M., Seifert, B., Sanabria, J., Argüello, G.L., 2009. Chronology of Late Pleistocene Pampa loess from the Córdoba area in Argentina. Journal of Quaternary Science 24 (7), 761–772.
Freytenet, P., 1971. Paleosols résiduels et paleosol alluviax hydromorphes dan le Crétace superieur e l'Eocène basal en Languedoc. Revue Géographie Physique et Geologie Dynamique 13, 245–268.
Imbrie, J., Boyle, E.A., Clemens, S.C., Duffy, A.W., Howard, R., Kukla, G., Kutzbach, J., Martinson, D.G., McIntyre, A., Mix, A.C., Molfino, B., Morley, J.J., Peterson, L.C., Pisias, N.G., Prell, W.L., Raymo, M.E., Shackleton, N.J., Toggweiler, J.R., 1992. On the structure and origin of major glaciation cycles, 1, linear responses to Milankovitch forcing. Paleoceanography 7, 701–738.
Jansen, E., Overpeck, J., Briffa, K.R., Duplessy, J.C., Joos, F., Masson-Delmontte, V., Olago, D., Otto-Bliesner, B., Peltier, W.R., Rahmstorf, S., Ramesh, R., Raynaud, D., Rind, D., Palomina, O., Villalba, R., Zhang, D., 2007. Palaeoclimate. In: Solomon, S., Qin, D., Manning, M., Chen, Z., Marquis, M., Averyt, K.B., Tignor, M., Miller, H.L. (Eds.), Climate 2007: The Physical Science Basis. Contribution of Working Group I to the Fourth Assessment Report of the Intergovernmental Panel on Climate Change. Cambridge University Press, Cambridge, United Kingdom/New York. http://ipcc-wgl.ucar.edu/wgl/Report/AR4WG1_Pub_Ch06.pdf.
Jin, Z.D., Wu, Y., Zhang, X., Wang, S., 2005. Role of late glacial to mid-Holocene climate in catchment weathering in the central Tibetan plateau. Quaternary Research 63, 161–170.
Kemp, R.A., Zárate, M., Toms, P., King, M., Sanabria, J., Arguello, G., 2006. Late quaternary paleosols, stratigraphy and landscape evolution in Nothern Pampa, Argentina. Quaternary Research 66, 119–132.
Khadkikar, A.S., Chamyal, L., Ramesh, R., 2000. The character and genesis of calcrete in Late Quaternary alluvial deposits, Gujarat, western India, and its bearing on the interpretation of ancient climates. Palaeogeography, Palaeoclimatology, Palaeoecology 162, 239–261.
Klappa, C.F., 1980. Rhizoliths in terrestrial carbonates: classification, recognition, genesis and significance. Sedimentology 27, 651–660.
Köppen, W., 1923. Die Klimate der Erde. Grundriss der Klimakunde, Berlin und Leipzig, X, 369 pp.
Mack, G., James, W., 1992. Calcic paleosols of the plio-pleistocene camp rice and Palomas formation, southern Río Grande rift, USA. Sedimentary Geology 77, 89–109.
Mack, G., James, W., 1994. Paleoclimate and the global distribution of paleosols. Journal of Geology 102, 360–366.
Miall, A.D., 1996. The Geology of Fluvial Deposits. Springer-Verlag, Berlin, 582 pp.
Nabel, P., Cione, A., Tonni, E., 2000. Environmental changes in the Pampean area of Argentina at the Matuyama-Brnhes (C1-C1n) Chrons boundary. Palaeoceanography, Palaeoclimatology, Palaeoecology 162, 403–412.
Orgeira, M.J., Pereyra, F., Vásquez, C., Castañeda, E., Compagnucci, R., 2008. Rock magnetism in modern soils, Buenos Aires province, Argentina. Journal of South American Earth Science 26, 217–224.
Quidelleur, X., Valet, J.P., 1994. Paleomagnetic records of excursions and reversals: possible biases caused by magnetization artefacts. Physics of the Earth and Planetary Interiors 82, 27–48.
Siddall, M., Chappell, Potter, E.K., 2007. Eustatic sea level during past interglacial. In: der Meer, Jaap J.M. (Ed.), The climate of past interglacial. Developments in Quaternary Science 7, 615 (Chapter 7).
Stoops, G., 2003. Guidelines for Analysis and Description of Soil and Regolith Thin Sections. Soil Science Society of America, Madison, Wisconsin, USA. 184 pp.
Stoops, G., Jongerius, A., 1975. Proposal for a micromorphological classification of soil materials. I. A classification of related distribution of coarse and fine particles. Geoderma 19, 247–249.
Tandon, S., Narayan, D., 1981. Calcrete conglomerate, case – hardened conglomerate and cornstone, Siwalik Group, Punjab, India. Sedimentology 28, 353–367.
Valencio, D.A., Orgeira, M.J., 1983. La magnetoestratigrafía del Ensenadense y Bonaerense de la Ciudad de Buenos Aires: Parte II. Revista de la Asociación geológica Argentina 38 (1), 21–33.
Visher, G.S., 1969. Grain size distributions and depositional processes. Journal of Sedimentary Petrology 39 (3), 1074–1106.
Winter, A., Paul, A., Nyberg, J., Oba, T., Lundberg, J., Schrag, D., Taggart, B., 2003. Orbital control of low-latitude seasonality during the Eemian. Geophysical Research Letters 30 (4), 1163.
Wright, V.P., 1990. A micromorphological classification of fossil and recent calcic and petrocalcic microstructures. In: Douglas, L. (Ed.), Soil Micromorphology: A Basic and Applied Science. Development in Soil Science 19, 401–407.
Wright, V.P., Tucker, M.E., 1991. Calcretes: an introduction. In: Wright, V.P., Tucker, M.E. (Eds.), Calcretes. International Association of Sedimentologists, Oxford, pp. 1–22. Reprint series.
Wright, V.P., Platt, N.H., Marriot, S.B., Beck, V.H., 1995. A classification of rhizogenic (root-formed) calcretes, with examples from de upper Jurassic-lower carboniferous of Spain and Upper Cretaceous of southern France. Sedimentary Geology 100, 143–158.
Zárate, M., 2003. Loess of southern south America. Quaternary Science Reviews 22, 1987–2006.
Zárate, M., Kemp, R., Blasi, A., 2002. Identification and differentiation of pleistocene paleosols in the northern Pampas of Buenos Aires, Argentina. Journal of South American Earth Science 15, 303–313.
Zárate, M., Kemp, R., Toms, P., 2009. Late quaternary landscape reconstruction and geochronology in the northern Pampas of Buenos Aires province, Argentina. Journal of South American Earth Science 27, 88–99.
Zárate, M., Orgeira, M.J. Sedimentación y edades magnéticas del cenozoico tardío continental de Argentina. En Escenarios de cambio ambiental: registros del Cuaternario en América Latina. Ed. Fondo de Cultura Económico por iniciativa de la Universidad Nacional Autónoma de México (UNAM) y Unión Mexicana de Estudios del Cuaternario (UMEC), in press.